Effects of ^{3}He impurity on solid ^{4}He studied by compound torsional oscillator

P. Gumann,[*] M. C. Keiderling, D. Ruffner, and H. Kojima

Serin Physics Laboratory, Rutgers University, Piscataway, New Jersey 08854, USA

Frequency shifts and dissipation of a compound torsional oscillator induced by solid ^{4}He samples containing ^{3}He impurity concentrations ($x_3 = 0.3, 3, 6, 12,$ and 25 in units of 10^{-6}) have been measured at two resonant mode frequencies ($f_1 = 493$ and $f_2 = 1164$ Hz) at temperatures (T) between 0.02 and 1.1 K. The fractional frequency shifts of the f_1 mode were much smaller than those of the f_2 mode. The observed frequency shifts continued to decrease as T was increased above 0.3 K, and the conventional nonclassical rotation inertia fraction was not well defined in all samples with $x_3 \geqslant 3$ ppm. Temperatures where peaks in dissipation of the f_2 mode occurred were higher than those of the f_1 mode in all samples. The peak dissipation magnitudes of the f_1 mode were greater than those of the f_2 mode in all samples. The activation energy and the characteristic time (τ_0) were extracted for each sample from an Arrhenius plot between mode frequencies and inverse peak temperatures. The average activation energy among all samples was 430 mK, and τ_0 ranged from 2×10^{-7} s to 5×10^{-5} s in samples with $x_3 = 0.3 - 25$ ppm. The characteristic time increased with increasing x_3. Observed temperature dependencies of dissipation were consistent with those expected from a simple Debye relaxation model if the dissipation peak magnitude was separately adjusted for each mode. Observed frequency shifts were greater than those expected from the model. The discrepancies between the observed and the model frequency shifts increased at the higher frequency mode.

I. INTRODUCTION

The discovery[1] that the resonant frequencies of torsional oscillators (TOs) containing solid ^{4}He samples increased at temperatures below about 300 mK has stirred much excitement (see reviews, Refs. 2–4). Interpreted as a partial decoupling or so-called[5] "non-classical rotational inertia (NCRI)" of the solid ^{4}He samples, the discovery gave evidence for the long-sought[6] supersolid state of solid ^{4}He simultaneously possessing crystallinity and superfluid properties. In the temperature range where the observed TO frequency shifts vary most rapidly, peaks in the energy dissipation of the TO are also observed. The frequency shifts and the accompanying dissipation of TO have been confirmed in many laboratories.[7–11] However, the interpretation in terms of supersolid state in the loaded solid ^{4}He samples remains controversial and a comprehensive understanding of the TO frequency shifts and other related phenomena in quantum solid ^{4}He at low temperatures has not been established.

There are puzzling observations in experiments designed to test the supersolid interpretation. Superflows that would be expected to occur through supersolid ^{4}He samples under applied pressure gradients have not been observed in the earlier flow experiments[12–14] carried out in the same temperature range as the NCRI effect is observed. Recently, however, unusual mass flows[15,16] were induced through solid ^{4}He samples below about 0.6 K by applying chemical potential gradients across the samples. Propagation of a fourth sound that would be expected for a superfluid has not been detected.[17,18] The shear modulus of a thin solid ^{4}He slab was found[13] to "stiffen" in a very similar manner as the frequency of TO containing an annular solid ^{4}He sample was found[1] to increase with decreasing temperature. This similarity indicated a common origin of these two effects. While almost none of these observations are clearly understood, it has become apparent that the details of the observations are affected strongly by the solid ^{4}He sample

quality depending on growth condition, sample geometry and size, and ^{3}He impurity. The objective of the present work is to gain understanding of the puzzling role played by ^{3}He impurity by use of our compound TO techniques.

The surprisingly high sensitivity of observed frequency shifts to minute ^{3}He impurity concentrations (x_3) at parts per million (ppm) levels in the ^{4}He samples has been reported by Kim *et al.*[1,19] The temperature dependence of the shear modulus was also found[13] to depend on x_3. On the other hand, a thermodynamic anomaly in heat capacity occurs at temperatures which are relatively insensitive to the value of x_3. The dynamics of ^{3}He atoms within solid ^{4}He may be probed by NMR experiments. Simultaneous observations of NMR and TO effects, of the same crystal, have been carried out by Toda *et al.*[20,21] in solid ^{4}He samples with x_3 down to 10 ppm. They found three different spin-lattice relaxation times, suggesting the existence of three different states of ^{3}He atoms in the solid matrix of ^{4}He. Kim *et al.*[22,23] reported their measurements of NMR relaxation times, T_1 and T_2, of ^{3}He contained in solid ^{4}He samples with x_3 down to 16 ppm. The relation between all of these NMR observations and the role of ^{3}He impurity in the supersolid phenomenon is yet to be clarified.

One goal of our work is to measure how the dissipation accompanying frequency shifts of solid-^{4}He-loaded TO depend on the amount of added ^{3}He impurity. The earlier reports[1,19] focused mainly on the variation of frequency shifts as x_3 was changed. Another goal is to measure how the dependence of frequency shifts and dissipation on the TO frequency varies as x_3 is changed. Frequency dependence studies are difficult in single-resonance-mode TOs. We report on the first[24] systematic measurements of the dependence of dissipation and frequency shifts on x_3 ($0.3 \sim 25$ ppm) using our compound TO having two resonance mode frequencies (~ 500 and ~ 1200 Hz). Unlike in the earlier ^{3}He impurity dependence study,[19] all samples are grown in the same torsional oscillator

following nearly identical solid growth procedures such that variance due to sample cell geometry and sample quality would be minimized. Measurements are made simultaneously at the two frequencies under identical sample conditions, and they allow us to explore dynamical effects which cannot be probed in a single-mode TO. For a given sample, the maximum in dissipation of the higher frequency mode appears at a higher (peak) temperature than the lower frequency mode. As x_3 is increased, the peak temperatures for both modes increase. Arrhenius plots of the mode frequencies vs inverse peak temperatures are analyzed to extract the activation energy and the characteristic time involved in the dissipation process. A simple form of Debye dissipation combined with the extracted characteristic time is inadequate to represent the observed frequency-dependent dissipation of the two modes separately. The frequency shifts expected from the dissipation by the Kramers-Kronig relation cannot account for those observed in the two modes. The limiting characteristic time τ_0 extracted from the two modes varies in proportion to $x_3^{2/3}$.

II. EXPERIMENT

Our compound torsional oscillator shown in Fig. 1 was modified from the earlier one[10,25] and has two torsion rods (a,b), each with diameter 1.9 mm and length 15 mm, and two interconnected masses. The flange above the upper rod (a) is rigidly attached to a large copper vibration isolation block in good thermal contact with the mixing chamber of a dilution refrigerator. The upper mass is a "dummy" comprised of a central disk (c) and two electrode fins (d) made of aluminum plates. The TO is capacitively driven by applying dc-biased sinusoidal voltage between a stationary electrode (not shown) and one of the movable electrode fins. The motion of the TO is detected by measuring the voltage induced between the
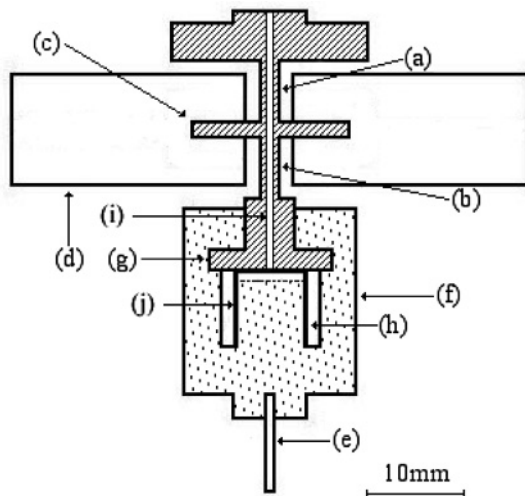

FIG. 1. Schematic of compound torsional oscillator. (a) upper torsion rod, (b) lower torsion rod, (c) upper disk, (d) electrode fins, (e) lower electrode fin, (f) cell body, (g) base, (h) annular sample chamber, (i) fill hole, and (j) copper foil liner. The shaded region is machined from a single block of BeCu. The width of the annular sample space is 1.0 mm but it is exaggerated here for clarity.

other electrode fin biased against another stationary electrode (not shown). The lower fin (e) acts as an auxiliary electrode for measuring the motion of the sample chamber itself. The lower mass (f) is mostly made of Stycast 1266 epoxy[26] cast around the base (g) below the lower torsion rod. The sample chamber (h) for solid ^{4}He is an annular space (8.0 mm inner diameter, 10.0 mm outer diameter, and 8.0 mm height). Helium is introduced into the chamber via the fill hole (i) drilled (diameter $= 0.8$ mm) through the center of torsion rods and the base, and a diametrical channel just below the lower surface of the base. To improve the thermal contact between the sample helium and the mixing chamber, the lower surface of the BeCu base is pressed against a 100-μm-thick copper foil (j) which is extended onto the inner wall of the sample space.

The ^{3}He impurity concentration is increased by adding a calibrated amount of ^{3}He gas into the cell prior to loading it with the commercial ultrahigh-purity ^{4}He (nominal $x_3 = 0.3$ ppm) at 4.2 K to approximately 80 bar. A solid sample is subsequently grown by the blocked capillary method. The solid plug formed in the rapidly cooled portion of the filling capillary maintains a constant mass in the sample space below the plug. A Straty-Adams capacitive pressure sensor attached to the isolation block is used to monitor the pressure in the fill tube during sample solid formation. The measured freezing temperature where a sudden increase in the oscillation amplitude occurs gives the pressure in the solid formed. After the plug is formed, the total time elapsed to freeze ^{4}He in the sample chamber is about 40 minutes for all the samples reported here. Since the sample solid pressure is 40 bar or greater, where the freezing temperature is higher than the highest superfluid ^{4}He transition temperature, redistribution of ^{3}He by the heat flush effect is expected to be unimportant. Upon completion of measurements for a given sample, the dilution refrigerator system is warmed up to near 6 K for pumping out helium from the cell. The pressure and the TO resonant frequencies are monitored during this "bake-out" procedure to ensure that the remaining residual amount of helium gas is sufficiently small. Subsequent to this procedure, another calibrated amount of ^{3}He is added such that the ^{3}He impurity concentration is larger than the previous sample and the above procedure is repeated to grow the next solid sample. In all, measurements were made on solid ^{4}He samples with $x_3 = 0.3$, 3, 6, 12, and 25 ppm. The samples are identified by their ^{3}He impurity concentrations. The uncertainty in x_3 is estimated to be $\pm 20\%$.

Sample temperature (T) is inferred from a ruthenium oxide resistance thermometer attached to the isolation block and is calibrated against a ^{3}He melting pressure thermometer. Reproducibility of the ruthenium oxide thermometer upon cycling up to room temperature is verified with a fixed point superconducting standard down to 15 mK.

The two modes of the compound TO may be excited and detected simultaneously. The resonant frequency and the amplitude of each mode are tracked continuously and independently by two automatic phase-lock feedback data acquisition systems. In all of the data presented in this report, measurements of both modes are taken simultaneously to ensure identical sample conditions. The drive levels are set such that sample velocity amplitude of each mode is less than about 15 μm/s. It has been found that effects of "critical

velocity" and hysteretic behavior are small at these low-velocity amplitudes. The shifts in frequency and amplitudes of the modes can strongly affect each other if the drive levels are increased beyond some threshold velocity.[27]

Prior to loading the cell with a sample solid, the "background" characteristics of the TO with no helium in the sample chamber are measured during slow ($\sim$15 mK/h) cooling and verified for reproducibility by following the temperature dependence of the resonant frequencies $f_{ib}(T)$ and the oscillation amplitudes $A_{ib}(T)$ of both modes ($i = 1, 2$). The background quality factor $Q_{ib}(T)$ is computed from the tracked oscillation amplitude via $Q_{ib}(T) = [A_{ib}(T)/A_{ib}(T_b)]Q_{ib}(T_b)$, where the reference quality factor $Q_{ib}(T_b)$ is determined from measured exponential ring downtime (reproducible within 10%) at $T_b \approx$ 200 mK.

Background characteristics measured at $T = 30$ mK are f_{1b} = 493 Hz, f_{2b} = 1164 Hz, $Q_{1b} \sim 7.7 \times 10^5$, and $Q_{2b} \sim 4.7 \times 10^5$. The observed background frequencies are in agreement within $\sim$12% with those computed from estimated moments of inertia and torsion constant of the rods.

After a sample of solid ^{4}He is grown as described above, the resonant frequencies decrease due to the added moment of inertia. "Loading frequency" Δf_i^0 in the "zero" temperature limit is defined as $\Delta f_i^0 \equiv f_{ib} - f_{is}$ corresponding to the decrease in the mode frequency from the background to sample-filled cell measured near 30 mK. The measured values are $\Delta f_1^0 = 0.40$ Hz and and $\Delta f_2^0 = 1.20$ Hz for the $x_3 = 0.3$ ppm sample shown in Fig. 2. These values are within 10% of those estimated from the added inertia of solid ^{4}He in the sample chamber. The variation in Δf_i^0 from sample to sample is less than 3%.
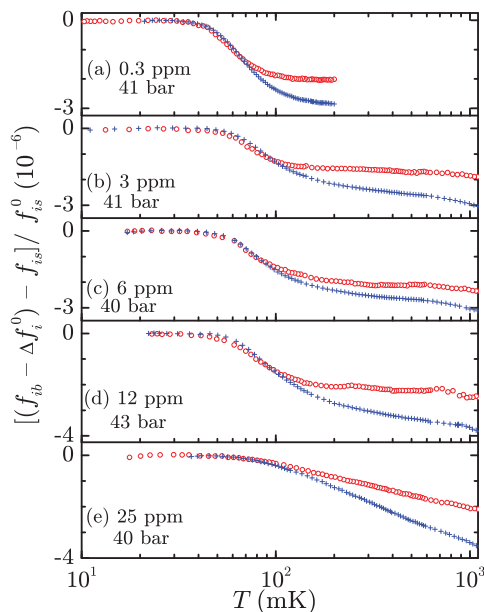

FIG. 2. (Color online) Temperature dependence of reduced frequency shift of the compound torsional oscillator with annular sample chamber: first mode [(red) open circles] and second mode [(blue) pluses]. Panels (a) $\sim$ (e) show results of solid ^{4}He samples containing ^{3}He impurity concentration of 0.3, 3, 6, 12, and 25 ppm, respectively. Indicated solid pressures are estimated from the loading liquid pressure at 4.2 K.

After a solid ^{4}He sample is grown in the cell, the same procedure as in the background characterization including the drive levels is followed to measure $f_{is}(T)$, $A_{is}(T)$, $Q_{is}(T_b)$, and $Q_{is}(T)$. The sample is warmed up at most to 300 mK in the $x_3 = 0.3$ ppm sample, to 1.1 K in the 3, 6, and 12 ppm samples, and to 2.0 K in the 25 ppm sample. Each sample data set is taken over about a 24-hour period while cooling to $\sim$20 mK from 250 mK in the 0.3-ppm sample and from 1 K in all other samples. The measured temperature dependence of $f_{is}(T)$ and $A_{is}(T)$ does not vary significantly from one temperature sweep to another if the maximum temperature is within these limits.

III. RESULTS

A. Frequency shift

Our results on frequency shifts are presented in Fig. 2 as "reduced frequency shifts" defined for each mode i as

$$\delta f_i(T)/f_{is}^0 \equiv \frac{\left[\left(f_{ib}(T) - \Delta f_i^0\right) - f_{is}(T)\right]}{f_{is}^0}, \quad (1)$$

where f_{is}^0 is the frequency of loaded TO at our minimum temperature (about 15 mK) depending on x_3. In the zero temperature limit the reduced frequency shift vanishes by definition. It remains, in all samples, at the zero temperature limit below about 40 mK and its magnitude monotonically increases at higher temperatures for both modes. Except in the $x_3 = 0.3$ ppm sample, temperature dependence of the reduced frequency shift of the first mode coincides with that of the second mode below about 100 mK. At temperatures greater than 100 mK changes in reduced frequency of the second mode are greater than those of the first mode. In all samples, except possibly the 0.3-ppm sample, the reduced frequency shifts for both modes continue to decrease as temperature is increased above 200 mK. The lack of data in the 0.3-ppm sample prevents us from making a firm statement about the temperature dependence of the reduced frequency shift above 200 mK in this sample.

The temperature range 50 mK $\lesssim T \lesssim$ 150 mK, where relatively rapid changes in the reduced frequency shift occurs in Fig. 2, has been identified as a signature of the occurrence of NCRI phenomenon. The reduced frequency shifts would become constant if the observed temperature dependence of $f_{is}(T)$ matched that of $f_{ib}(T)$ at temperatures greater than some "onset" temperature where the fraction of solid sample apparently decoupled from the container, or NCRI fraction (NCRIf), vanishes. Such matching was not found at the low drive levels applied to our TO. Since identifying onset temperatures in our samples is ambiguous, reduced frequency shifts rather than NCRIf are shown in Fig. 2.

The reduced frequency shift in the 25-ppm sample shows qualitatively distinct behavior from other samples. In comparison to other samples, there is no temperature range where the reduced frequency shifts vary relatively more rapidly. At temperatures roughly above 150 mK, the frequency shifts decrease linearly (on the logarithmic temperature scale), with the second mode having larger slope than the first. Measured dissipation in the 25-ppm sample is also distinct from other samples (see Fig. 3).
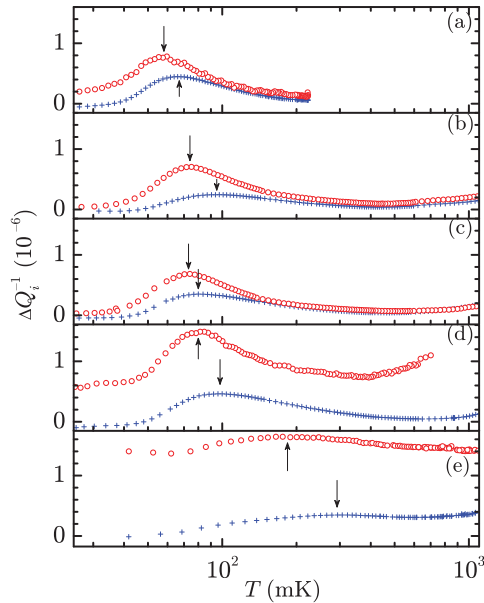
FIG. 3. (Color online) Temperature dependence of the change in dissipation from empty to loaded sample chamber: first mode [(red) open circles] and second mode [(blue) pluses]. Measurements are taken simultaneously with those reduced frequency shifts in the samples (with the same panel designations for ^{3}He impurity concentration) as shown in Fig. 2. Arrows indicate temperatures where peaks in dissipation occur.

B. Dissipation

The change in dissipation of each mode produced by loading solid ^{4}He samples is computed by taking the difference:

$$\Delta Q_i^{-1}(T) = Q_{is}^{-1}(T) - Q_{ib}^{-1}(T). \quad (2)$$

Evaluated temperature dependence of $\Delta Q_i^{-1}(T)$ is displayed in Fig. 3 for each sample shown in Fig. 2. Samples with $x_3 \leqslant$ 12 ppm have similar temperature dependence with $\Delta Q_i^{-1}(T)$ passing through local maxima at "peak temperatures" (T_{ip}) indicated by arrows in Fig. 3. Locating T_{ip} is aided and supported by the similarity of the changes in dissipation being plotted against T_{ip}/T among all samples (see Fig. 5). The 25-ppm sample shows broader temperature dependence than the other samples. The change in dissipation of the first mode is greater than that of the second in all samples. This is in contrast to the reduced frequency shift of the second mode being greater than that of the first in all samples at temperatures above 100 mK (see Fig. 2). At temperatures below 40 mK, ΔQ_2^{-1} for some samples is negative. This peculiar feature may have resulted in part from an uncertainty ($\sim$10%) in the measurements of reference quality factors and from small inaccuracy in the cell temperature measurement below 40 mK. Small temperature gradients between the sample and the thermometer could lead to errors in taking the difference between the two measurements with the sample chamber being empty and loaded.

The observed frequency-dependent peak temperature that the compound TO technique uniquely yields is an important parameter in considering the dynamical effects occurring in the oscillating ^{4}He samples. The peak temperatures are fairly well
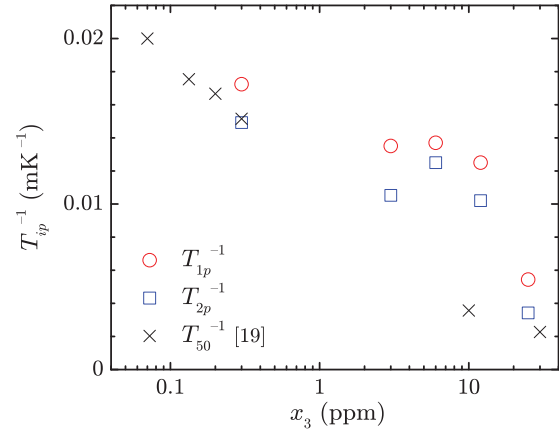

FIG. 4. (Color online) Inverse of dissipation peak temperature vs ^{3}He impurity concentration: first mode [(red) circles] and second mode [(blue) squares]. "Half-maximum temperatures" or T_{50} (crosses) are taken from Kim et al.[19]

defined, except in the 6- and 25-ppm samples whose ΔQ_2^{-1} are broader than the others. The inverse of the peak temperature of the two modes in each sample is shown in Fig. 4. It can be seen that $T_{p2} > T_{p1}$ in all samples. This frequency dependence of the peak temperature was also found in a cylindrical sample chamber geometry in solid ^{4}He with nominal 0.3-ppm ^{3}He concentration[10] and appears to be independent of sample geometry and size (down to 0.2 mm), ^{3}He concentration, and sample growth conditions. The peak temperature generally increases for both modes as x_3 is increased. An apparent plateau in T_{ip} in the range 3 ppm $< x_3 <$ 10 ppm is likely caused by some accidental variation in an as-yet-unidentified source of dissipation in the sample characteristics. It is interesting to note that the "half-maximum temperature" (T_{50}), where Kim et al.[19] found NCRIf to decrease to half of the maximum at the lowest temperatures, smoothly extends the dependence of T_{ip} on x_3 found here.

The same results as shown in Fig. 3 are replotted in Fig. 5 by normalizing the inverse temperature as T^{-1}/T_{ip}^{-1} and the dissipation as $\Delta Q_i^{-1}/\Delta Q_i(T_{ip})^{-1}$. Plotting in this manner reveals similarity and dissimilarity among the samples with varying ^{3}He impurity concentration. The normalized dissipation for the first mode in the 12- and 25-ppm samples and the second mode in the 25-ppm sample deviate considerably from others. The "sharp" increases in the normalized dissipation at high temperatures, $T_{ip}/T \lesssim 0.2$ (first mode) and 0.4 (second mode), become accentuated in Fig. 5. Deviations in the samples with higher x_3 from the other bell-shaped dependence on T_{ip}/T indicate an emergence of nearly temperature-independent "extra" dissipation.

Annealing of solid ^{4}He samples has been found[7,9,28] to affect the frequency shift and dissipation in TO experiments. Possible effects of sample "annealing" were studied in our $x_3 =$ 0.3 ppm sample by raising the temperature of the cell to 1.8 K (below the melting temperature of the sample) and maintaining the temperature for 10 hours. The temperature is then reduced to 0.3 K over six hours. Subsequently measured temperature dependence of the frequency shifts of the two modes are similar to those shown in Fig. 2, except f_{is}^0 decreases by 7.2 and 21.5 mHz for $i = 1$ and 2, respectively. This observation is
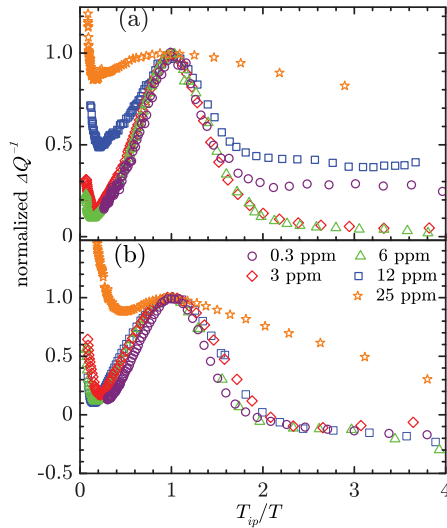
FIG. 5. (Color online) Normalized (see text) change in dissipation: first mode [panel (a)] and second mode [panel (b)] of all samples shown in Fig. 3. Symbols: (purple) circles (x_3[ppm] = 0.3), (red) lozenges (3), (green) triangles (6), (blue) squares (12), and (orange) stars (25). Results shown for the 25-ppm sample include temperatures up to 2.5 (1.6) K for the first (second) mode not displayed in Fig. 3.

contrary to that of the recent experiment,[28] which finds that the measured frequency shift at lowest temperatures is not affected by annealing. The dissipation peak temperatures decrease by about 5 mK after annealing. Our annealing process decreases the extracted (see Sec. IV) characteristic time slightly but produces no significant change in the activation energy.

IV. ANALYSIS

The original discovery[1] of frequency shifts at low temperatures in TOs loaded with solid ^{4}He and all subsequent confirmations, to our knowledge, have been accompanied by dissipation having puzzling resonancelike temperature dependence as exemplified by panel (a) in Fig. 3. In this section we analyze the observed dependence of dissipation and frequency shifts on ^{3}He impurity concentration in solid ^{4}He samples. It is generally agreed that dissipation peaks occur at temperatures where an internal dynamical rate (τ^{-1}) matches the imposed TO frequencies (ω_i), or where $\omega_i \tau = 1$. The internal dynamics of vortex motion,[29] glassy response,[30] superglass,[11,31] presence of tunneling two-level systems,[32] and viscoelastic behavior[33] have been suggested as the physical origin of dissipation. The vibration of dislocation line segments pinned at network nodes and by ^{3}He impurity has also been suggested[34] as the origin of the observed TO behavior.

Assuming that the internal dynamics is thermally driven, we consider a simple, activated dynamical time τ given by the Arrhenius form

$$\tau = \tau_0 \exp \frac{E_0}{k_B(T - T_0)}, \qquad (3)$$

where k_B is the Boltzmann constant, τ_0 a characteristic time, and E_0 an activation energy. A possibly nonvanishing

"transition temperature" T_0 is introduced in Eq. (3) for generality, but we assume $T_0 = 0$ in our analysis for simplicity. To examine our dissipation results in terms of Eq. (3), the mode frequencies are plotted in Fig. 4 on a logarithmic scale at corresponding T_{ip}^{-1} in each sample. The slopes and the intercepts determined strictly by straight lines (*not* shown) connecting the two points for each sample in Fig. 6 are $(E_0/k_B[\text{mK}], \tau_0[\text{s}]) = (380, 5 \times 10^{-7}), (290, 7 \times 10^{-6}), (720, 2 \times 10^{-8}), (370, 3 \times 10^{-6}),$ and $(430, 3 \times 10^{-5})$ for $x_3 = $ 0.3-, 3-, 6-, 12-, and 25-ppm samples, respectively. Broadness in the dissipation peaks introduces considerable uncertainties (indicated by error bars in Fig. 6) in the values of T_{ip} and leads to scattering in these values of E_0/k_B and τ_0^{-1}. The tendency in Fig. 6, however, suggests that E_0 is a constant independent of x_3. To make progress, let us assume that $E_0/k_B = $ 430 mK, the average of the above slopes, is a good estimate for the activation energy. It is interesting to note that this average activation energy is close to the binding energy of ^{3}He dislocation lines found in the analysis of their experiments by Kim *et al.*[19] and Day and Beamish.[13]

The intercepts of the best fits (shown by a straight line for each x_3 sample in Fig. 6) with the set slope specify the values of τ_0 as shown in Fig. 7. There is a trend for τ_0 to increase as x_3^γ, where $\gamma \sim 2/3$ if $x_3 < 20$ ppm. Both the reduced frequency shifts and dissipation of the 25 ppm sample show qualitatively different behaviors than the samples with lower ^{3}He impurity concentration. The fitted exponent γ becomes $1 \sim 1.2$ if the 25-ppm data point in Fig. 7 is included. It appears that τ_0 also changes its dependence on x_3 beyond $20 \sim 25$ ppm. It was already noted that the values of T_{50} measured by single-frequency TO techniques by Kim *et al.*[19] are fairly close to T_{ip} (see Fig. 4). Constraining straight lines with the same slope as shown in Fig. 6 by their TO frequencies at T_{50}^{-1} implies values of τ_0 as shown in Fig. 7 for their samples. Considering differences in sample chamber geometry, sample growth process, measurement methods, etc., τ_0 extracted from the T_{50} data of Kim *et al.*[19] overlaps and fits surprisingly well
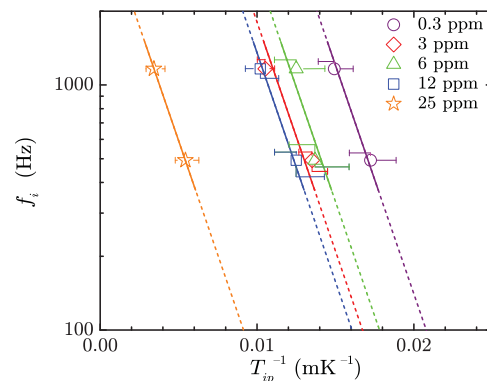

FIG. 6. (Color online) Torsional oscillator frequencies plotted at inverse temperatures where dissipation peaks occur in solid ^{4}He samples with given ^{3}He impurity concentrations. All straight lines have the same slope corresponding to an activation energy E_0 of 430 mK and have ordinate intercepts which are adjusted for best fit for each sample. The intercepts represent the characteristic dynamic rate τ_0^{-1} (see text). Symbols for samples with different values of x_3 are same as those in Fig. 5.
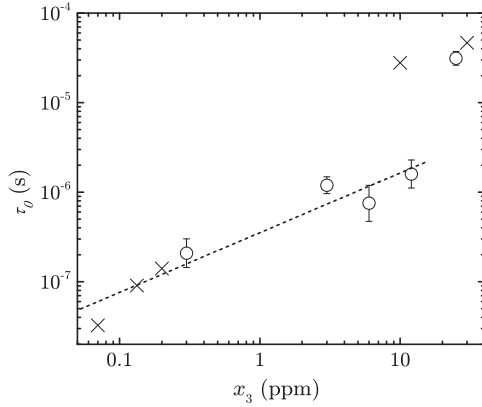
FIG. 7. Characteristic time τ_0 vs ^{3}He impurity concentration. The values of τ_0 are determined by the intercepts of the straight lines in Fig. 6. The dashed line represents $\tau_0 = 3.5 \times 10^{-7} x_3^{2/3}$ s (see Discussion section of text). Crosses show τ_0 calculated from the T_{50} data of Kim *et al.*[19] using the same activation energy as in Fig. 6 and their TO frequencies (see text).
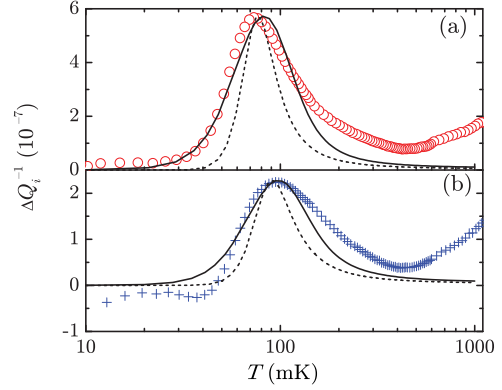

FIG. 8. (Color online) Comparison of dissipation in the 3-ppm sample with the dissipation expected from Debye susceptibility. Same data as shown in Fig. 3 are repeated for mode 1 [(red) circles] and 2 [(blue) pluses] in panels (a) and (b), respectively. In each panel, curves are dissipation expected (see text) from Eq. (5): assuming single activation energy and $\tau_0 = 1.2 \times 10^{-6}$ s and from Eq. (7) (dashed curves), and allowing Gaussian distribution of activation energy with $w/k_B = 120$ mK and from Eq. (8) (solid curves).

with extrapolation of our results to lower values of x_3. Clearly it is of interest to extend frequency-dependence studies like ours to smaller ^{3}He impurity concentration than we have carried out.

The mechanical response of driven TOs containing solid ^{4}He samples has been treated[30] by including a general form of rotational susceptibility to account for the sample motion:

$$\chi = \frac{2G}{1 - (j\omega_i \tau)^\beta},\tag{4}$$

where G is a constant (possibly dependent on frequency[35]), ω_i is angular frequency, τ is a relaxation time, and β is an exponent dependent on a particular model. Including the general susceptibility results in extra dissipation and concomitant frequency shifts in the TO response. In our simplified analysis, the "Debye model" response is considered by assuming $\beta = 1$. In this case, the change in dissipation due to sample motion is given by

$$\Delta Q_i^{-1} = \frac{2G\omega_i \tau}{\left(1 + \omega_i^2 \tau^2\right)},\tag{5}$$

and the accompanying reduced frequency shift by

$$\frac{f_{is} - f_{ib} - \Delta f_i}{f_{is}^0} = -\frac{G}{\left(1 + \omega_i^2 \tau^2\right)}.\tag{6}$$

Although the linear response model assumed here may not be entirely applicable to our experiment, it is of interest to examine if the model can achieve a similar success as in the description[36] of the shear modulus measurements. Our results are compared with those expected from Eq. (5) by assuming the Arrhenius form of relaxation time characterized by our average activation energy and the extracted τ_0 as shown in Fig. 7. Dissipation extracted from the experiment and from the model are compared in Fig. 8 for the 0.3-ppm sample. The observed peak dissipation of the first mode at T_{1p} is significantly larger than that of the second mode at T_{2p}, in disagreement with the frequency-independent peak dissipation expected from Eq. (5). To proceed with the (modified) Debye model, the value of G is adjusted for each mode separately to match the peak

dissipation at T_{ip} in Fig. 8. Dissipation expected from the model produces narrower widths in temperature dependence around the peaks than those observed. Comparisons in other samples show similar deviations between the observations and the model. The model of course does not account for the upturns in dissipation at high temperatures nor for the low-temperature residual dissipation observed in 12- and 25-ppm samples.

As seen in Fig. 8, the observed temperature dependence of dissipation is broader than expected from the Debye model, assuming Arrhenius relaxation time with one activation energy for the system. Broader temperature dependence may be introduced into the model by allowing a distribution in the activation energy. A canonical Gaussian distribution $N(E)$ given by

$$N(E) = \frac{1}{\sqrt{2\pi w^2}} e^{-\frac{1}{2}\left(\frac{E - E_0}{w}\right)^2}\tag{7}$$

is applied to Eq. (5) to evaluate $\Delta \bar{Q}_i^{-1}$:

$$\Delta \bar{Q}_i^{-1}(T) = \int \Delta Q_i^{-1}(T, E) N(E) dE.\tag{8}$$

Here, E_0/k_B is set as the average activation energy and the width w of the distribution is adjusted for each sample. The peak dissipation value G is readjusted separately for each mode to match the respective peak dissipation. For the 3-ppm sample, adjusting to $w/k_B = 120$ mK can represent the data fairly well, as shown in Fig. 8. In the cases of 12- and 25-ppm samples, there appear residual amounts of dissipation at low temperature. In these two samples, a constant added to ΔQ_i^{-1} is taken as an additional fitting parameter. The width of distribution obtained from fitting the data in this manner is shown in Fig. 9. Values of w within the error bars shown in Fig. 9 give similar goodness of fit for both modes. Despite large uncertainties, a clear increasing trend in w is discernible as x_3 is increased. We suggest that temperature widths around
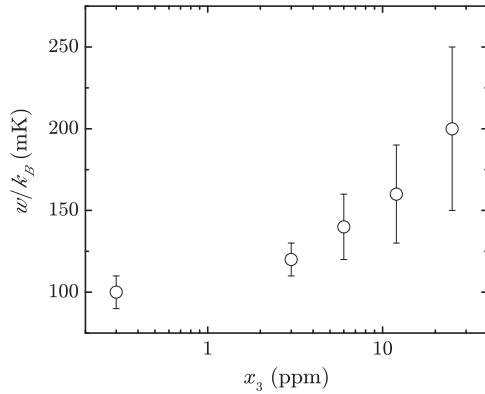
FIG. 9. Variation of width in distribution of activation energy. Widths are determined by fitting temperature dependence of dissipation in each sample using Eqs. (7) and (8) (see text).

the dissipation peaks in TO experiments can provide sample characterization in the distribution of activation energy.

Using the same respective parameter values in evaluating dissipation for each mode shown in Fig. 8, the frequency shifts expected from Eq. (6), with single and distributed activation energy, are shown in Fig. 10 for the 3-ppm sample. The expected frequency shift of the first mode by including distribution in the activation energy approaches the observed frequency shift but a considerable difference remains. The expected frequency shifts of the second mode are much smaller than the observed. The large discrepancy in the second mode occurs despite independently adjusting the value of G for this mode as described above. The observed decrease in dissipation *and* increase in reduced frequency shift as the TO frequency is increased is a major inconsistency with the modified Debye model above. The difference in reduced frequency shifts between the measured and the Debye model
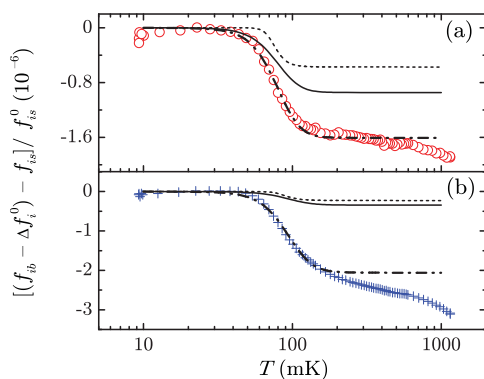

FIG. 10. (Color online) Comparison of $x_3 = 3$ ppm sample frequency shift data with those expected from Debye susceptibility using parameters determined from fitting the dissipation data as shown in Fig. 8. Dashed and solid curves are those expected from the dissipation shown in Fig. 8 with the single activation energy and with the distribution of activation energy, respectively. Dash-dotted curves are obtained by multiplying the solid curves of the respective modes by constants (see text). Same data (but depopulated for clarity) as shown in Fig. 2 are repeated for modes 1 [(red) circles] and 2 [(blue) pluses] in panels (a) and (b), respectively.

would be a consequence of a superfluidity in solid ^{4}He. A similar conclusion is made by Yoo and Dorsey[33] in the analysis of their viscoelastic model for solid ^{4}He.

Despite the clear distinction demonstrated in the reduced frequency shifts between the measured and the modified Debye model, similarity in temperature dependence between the two in Fig. 10 is evident. Multiplying the Debye expectations shown by solid curves for the first and second mode by constants, 1.7 and 6.0, respectively, gives temperature dependence shown by dash-dotted curves in Fig. 10. Except in high-temperature tail regions, the scaled temperature dependence matches the measured reduced frequency shifts quite well. Similar matching is seen in other samples with multiplicative constants applied to the first mode and second mode of (1.4, 3.5), (1.3, 3.9), and (1.25, 3.6) in 0.3-, 6-, and 12-ppm samples, respectively. The 25-ppm sample cannot be matched in a similar manner due to the large offset in dissipation. How this similarity in temperature dependence is related to the interpretation of supersolidity is not yet clear to us.

Nussinov *et al.*[30] and Graf *et al.*[37] have carried out much more sophisticated analyses of observed TO responses with generalized rotational susceptibilities expressing glassy response. They found that various single-frequency TO responses in both dissipation and frequency shift could be fitted by appropriately adjusting parameters in the glassy response model. Graf *et al.*[38] recently reported their study of the frequency dependence in the dissipation and frequency shifts observed[10] in our compound TO with a cylindrical sample chamber by allowing frequency dependence in the parameter G in Eq. (4). In our simple analysis of the observed ^{3}He impurity concentration-dependent effects in the present annular sample chamber, we restricted ourselves to the above-modified Debye model in which the value of G is *adjusted for each mode separately* to account for its apparent frequency dependence. Comparison of the cylindrical and annular sample chamber results indicates that the magnitude of frequency dependence of reduced frequency shifts increases as the sample chamber size is decreased.

V. DISCUSSION

It is noted that the extracted characteristic time shown in Fig. 7 varies almost in proportion to $x^{2/3}$ except for the 25-ppm sample. We speculate that this dependence stems from the diffusion process of ^{3}He condensed onto dislocation lines in solid ^{4}He samples. The diffusion time τ_d of ^{3}He along the dislocation lines may be approximated as $\tau_d \approx s^2/D$, where s is some characteristic distance over which ^{3}He moves during a time interval ω_i^{-1}, and $D \approx lv$ is a diffusion constant with mean-free path l and particle velocity v. Let us suppose that the mean-free path is approximately given by the effective dislocation loop length L. We follow Iwasa[39] in writing L as a parallel combination of the ^{3}He impurity length L_i and the network pinning length L_N:

$$L^{-1} = L_i^{-1} + L_N^{-1} \tag{9}$$

$$= \left[g x_3^{-\frac{2}{3}} \exp\left(-\frac{2W_0}{3T}\right) \right]^{-1} + L_N^{-1}, \tag{10}$$

where $g = 3.4 \times 10^{-7}$ (see Iwasa[34]) is a constant and W_0 is the binding energy of ^{3}He impurity to dislocation line. At low temperatures where L_i dominates over L_N, the characteristic time takes on the Arrhenius form

$$\tau_d = \frac{s^2}{g v} x_3^{2/3} \exp(E_0/T). \tag{11}$$

Identifying τ_d as τ and the coefficient on the right-hand side of Eq. (11) as τ_0, we expect it to depend on the impurity concentration as $\propto x_3^{2/3}$. Letting $s^2/v = 1.2 \times 10^{-9}$ cm s, $W_0/k_B (= 3E_0/2k_B) = 0.65$ K, and $L_N = 2$ μm (similar "fits" can be achieved for $1 \sim 5$ μm) gives the dependence on x_3 as shown by the dashed line in Fig. 7. This dependence appears to describe the observed dependence of τ_0 on x_3 except for the 25-ppm sample. Clearly more work is needed at additional impurity concentrations and larger ranges in torsional-oscillator frequency in order to firmly establish the power-law dependence of τ_0 on x_3.

There are questions that can be raised on the above diffusion process to describe the observed characteristic time τ_0 as x_3 is varied. If the mean-free path of a ^{3}He atom along a dislocation line is determined by other ^{3}He atoms condensed onto the dislocation line, it implies that ^{4}He atoms along the line mysteriously manage not to contribute to scattering. The process also implies that the diffusion coefficient of ^{3}He would *decrease* in the low-temperature limit as $\exp(-E_0/T)$. This temperature dependence is in contrast to the temperature-independent quantum diffusion coefficient of ^{3}He in bulk solid ^{4}He found by NMR experiments[40] above 0.55 K. The Kyoto group has observed very long spin-lattice relaxation in their NMR experiment on solid ^{4}He samples with $x_3 \approx 30$ ppm. The long relaxation time might be related to the decreasing D implied by our analysis.

Iwasa[34] has analyzed TO experiments and shear modulus shifts in terms of the Granato-Lücke model[41] on the interaction between an externally oscillated TO container and the induced vibrational motion of the dislocation lines present in the loaded ^{4}He solid sample. The analysis predicts shifting temperature dependence of the TO frequency and the dissipation peak temperature to higher temperatures as x_3 is increased, in general agreement with observations. However, since the expected natural vibration frequencies of the dislocation lines are much higher than the TO frequencies so far attempted, little frequency dependence is expected in both frequency shift and dissipation. This aspect of the model[34] is yet to be reconciled with our TO experiments.

Gaudio *et al.*[42] proposed a model[43] on the effects of ^{3}He on TO experiments where uniformly distributed ^{3}He impurities set the maximum grain size in solid ^{4}He samples. This model is not likely to be applicable in the range of values of x_3 in our experiments where ^{3}He atoms are expected to condense onto dislocation lines. Manousakis[44] considered ^{3}He impurity atoms binding to defects and promoting ^{4}He atoms to interstitial sites. It is not clear to us how this effect relates to the temperature-dependent changes in dissipation observed here as x_3 is varied.

Day and Beamish[13] discovered that temperature-dependent changes in the shear modulus of solid ^{4}He were almost identical to those in frequency shifts observed in TO experiments. The discovery gives strong impetus for concluding that the observed changes in shear modulus and frequency shift have similar physical origin. Syshchenko *et al.*[36] recently reported on their measurements of the changes in shear modulus and associated dissipation at frequencies between 0.5 Hz and 8 kHz. They analyze (see also Su *et al.*[45]) their data with a Debye relaxation process and thermally activated dynamics just as we do. When a distribution of activation energy is included, they find that the relationship between the shear modulus and the dissipation can be accounted for at different frequencies by the assumed Debye and thermal activation processes. This is in sharp contrast to the simplified analysis of our TO data: including distributions in activation energy cannot account for both frequency shifts and dissipation. The discrepancy increases at higher frequency (see Fig. 10).

VI. CONCLUSION

Effects of adding ^{3}He impurity to solid ^{4}He samples contained in an annular chamber were studied simultaneously at two resonant mode frequencies (differing by a factor of 2.4) by means of a compound torsional oscillator. Both frequency shifts and extra dissipation produced by the loaded samples were measured. Maxima in the measured dissipation occurred at impurity-concentration (x_3) dependent "peak temperatures" around which the frequency shifts varied more rapidly. When normalized to both the temperature and the dissipation level at the peak, the temperature dependence of dissipation became nearly universal in all samples studied, except in the 25-ppm sample. A thermal activation energy (430 mK) and characteristic relaxation times were extracted from Arrhenius plots of frequency versus the inverse of dissipation peak temperature. The characteristic time increased with impurity concentration approximately as $x_3^{2/3}$, suggesting diffusion of ^{3}He atoms along dislocation lines as the dynamical process producing the observed dissipation. Observed temperature dependence of dissipation of both modes could be fairly well described by a simple Debye model by allowing for Gaussian distribution of activation energy if the magnitude of dissipation at the peak temperature was allowed to be frequency dependent. The measured magnitudes of frequency shifts were significantly greater than those expected from the model, especially in the higher frequency mode. There remained "excess" amounts of frequency shifts which could not be accounted for by the simple Debye model. The excess frequency shifts may be attributed to superfluidity in solid ^{4}He at low temperatures. We believe that these frequency-dependent effects hold a key to understanding the dynamics of quantum solid ^{4}He.

*Present address: Institute for Quantum Computing, University of Waterloo, Ontario, Canada.

[1] E. Kim and M. Chan, Nature (London) **427**, 225 (2004); **305**, 1941 (2004).

[2] N. Prokof'ev, Adv. Phys. **56**, 381 (2007).

[3] S. Balibar and F. Caupin, J. Phys. Condens. Matter **20**, 173201 (2008).

[4] D. E. Galli and L. Reatto, J. Phys. Soc. Jpn. **77**, 1010 (2008).

[5] A. Leggett, Phys. Rev. Lett. **25**, 1543 (1970).

[6] M. Meisel, Physica B **178**, 121 (1992).

[7] A. S. C. Rittner and J. D. Reppy, Phys. Rev. Lett. **97**, 165301 (2006).

[8] M. Kondo, S. Takada, Y. Shibayama, and K. Shirahama, J. Low Temp. Phys. **148**, 695 (2007).

[9] A. Penzev, Y. Yasuta, and M. Kubota, J. Low Temp. Phys. **148**, 677 (2007).

[10] Y. Aoki, J. C. Graves, and H. Kojima, Phys. Rev. Lett. **99**, 015301 (2007).

[11] B. Hunt, E. Pratt, V. Gadagkar, M. Yamashita, A. V. Balatsky, and J. C. Davis, Science **324**, 632 (2009).

[12] D. S. Greywall, Phys. Rev. B **16**, 1291 (1977).

[13] J. Day and J. Beamish, Nature (London) **450**, 853 (2007).

[14] A. S. C. Rittner, W. Choi, E. J. Mueller, and J. D. Reppy, Phys. Rev. B **80**, 224516 (2009).

[15] M. W. Ray and R. B. Hallock, Phys. Rev. Lett. **100**, 235301 (2008).

[16] M. W. Ray and R. B. Hallock, Phys. Rev. Lett. **105**, 145301 (2010).

[17] Y. Aoki, H. Kojima, and X. Lin, Low Temp. Phys. **34**, 329 (2008).

[18] S. Kwon, N. Mulders, and E. Kim, J. Low Temp. Phys. **158**, 590 (2010).

[19] E. Kim, J. S. Xia, J. T. West, X. Lin, A. C. Clark, and M. H. W. Chan, Phys. Rev. Lett. **100**, 065301 (2008).

[20] R. Toda, P. Gumann, K. Kosaka, M. Kanemoto, W. Onoe, and Y. Sasaki, Phys. Rev. B **81**, 214515 (2010).

[21] R. Toda, W. Onoe, M. Kanemoto, T. Kakuda, Y. Tanaka, and Y. Sasaki, J. Low Temp. Phys. **162**, 476 (2011).

[22] S. S. Kim, C. Huan, L. Yin, J. Xia, D. Candela, and N. S. Sullivan, J. Low Temp. Phys. **158**, 584 (2010).

[23] S. S. Kim, C. Huan, L. Yin, J. Xia, D. Candela, and N. S. Sullivan, e-print arXiv:1012.3709.

[24] P. Gumann, D. Ruffner, M. C. Keiderling, and H. Kojima, J. Low Temp. Phys. **158**, 567 (2009).

[25] Y. Aoki, J. Graves, and H. Kojima, J. Low Temp. Phys. **150**, 252 (2008).

[26] Emerson and Cuming, Billerica, MA 01821.

[27] M. C. Keiderling, P. Gumann, D. Ruffner, and H. Kojima (to be published).

[28] J. D. Reppy, Phys. Rev. Lett. **104**, 255301 (2010).

[29] P. W. Anderson, Nat. Phys. **3**, 160 (2007); S. Shevchenko, Sov. J. Low Temp. Phys. **13**, 61 (1987).

[30] Z. Nussinov, A. V. Balatsky, M. J. Graf, and S. A. Trugman, Phys. Rev. B **76**, 014530 (2007).

[31] G. Biroli, C. Chamon, and F. Zamponi, Phys. Rev. B **78**, 224306 (2008).

[32] A. F. Andreev, JETP **109**, 103 (2009).

[33] C. D. Yoo and A. T. Dorsey, Phys. Rev. B **79**, 100504 (2009).

[34] I. Iwasa, Phys. Rev. B **81**, 104527 (2010).

[35] M. Graf, Z. Nussinov, and A. Balatsky, J. Low Temp. Phys. **158**, 550 (2010).

[36] O. Syshchenko, J. Day, and J. Beamish, Phys. Rev. Lett. **104**, 195301 (2010).

[37] M. J. Graf, A. V. Balatsky, Z. Nussinov, I. Grigorenko, and S. A. Trugman, J. Phys.: Conf. Ser. **150**, 032025 (2009).

[38] M. Graf, J.-J. Su, H. Dahal, I. Grigorenko, and Z. Nussinov, J. Low Temp. Phys. **162**, 500 (2011).

[39] I. Iwasa and H. Suzuki, J. Phys. Soc. Jpn. **49**, 1722 (1980).

[40] A. R. Allen, M. G. Richards, and J. Schratter, J. Low Temp. Phys. **47**, 289 (1982).

[41] A. Granato and K. Lücke, J. Appl. Phys. **27**, 583 (1956).

[42] S. Gaudio, E. Cappelluti, G. Rastelli, and L. Pietronero, Phys. Rev. Lett. **101**, 075301 (2008).

[43] B. Yucesoy, J. Machta, N. Prokofev, and B. Svistunov, Phys. Rev. Lett. **104**, 049601 (2010); S. Gaudio, E. Cappelluti, G. Rastelli, and L. Pietronero, ibid. **104**, 049602 (2010).

[44] E. Manousakis, Europhys. Lett. **78**, 36002 (2007).

[45] J.-J. Su, M. J. Graf, and A. V. Balatsky, Phys. Rev. Lett. **105**, 045302 (2010).